Nanoscale Spin Wave Localization Using Ferromagnetic Resonance Force Microscopy

Han-Jong Chia,[1,2,*] Feng Guo,[1,2] L. M. Belova,[3] and R. D. McMichael[1,†]

[1]Center for Nanoscale Science and Technology, National Institute of Standards and Technology, Gaithersburg, Maryland 20899, USA
[2]Maryland Nanocenter, University of Maryland, College Park, Maryland 20742, USA
[3]Department of Materials Science and Engineering, Royal Institute of Technology, 10044 Stockholm, Sweden

(Received 15 September 2011; published 24 February 2012)

We use the dipolar fields from a magnetic cantilever tip to generate localized spin wave precession modes in an in-plane magnetized, thin ferromagnetic film. Multiple resonances from a series of localized modes are detected by ferromagnetic resonance force microscopy and reproduced by micromagnetic models that also reveal highly anisotropic mode profiles. Modeled scans of line defects using the lowest-frequency mode provide resolution predictions of (94.5 ± 1.5) nm in the field direction, and (390 ± 2) nm perpendicular to the field.

DOI: 10.1103/PhysRevLett.108.087206 PACS numbers: 75.30.Ds, 75.70.Ak, 75.78.−n

The ability to manipulate ferromagnetism on submicron and nanometer length scales underpins the operation of commercial products including computer hard disc drives and magnetic random access memory (MRAM) chips. Ferromagnet dynamics are also at the heart of a wide array of devices currently under development or proposed for future electronics [1–8]. For these technologies, measurements that detect and image magnetization dynamics of individual nanostructures are desirable. In particular it would be highly useful to develop the ability to characterize the magnetic properties of buried devices, to measure device-to-device variations and ultimately, to measure magnetic property variations at different locations within individual devices.

Spin wave localization provides an avenue for achieving local magnetic property measurements. Unlike magnetic resonance imaging (MRI) in paramagnets [9] the strong exchange and dipolar interactions within ferromagnets generally preclude localizing precession using a simple field gradient [10]. However, localization can be achieved by trapping spin waves in regions of low internal field [11], and these internally localized modes have been used to characterize film edges in transversely magnetized stripe arrays [12–17], and ''end modes'' in dots of various shapes [18]. Spin waves can also be localized by an inhomogeneous externally applied field, such as the field from a magnetic cantilever tip [19–22]. The imaging capabilities of localized modes were demonstrated by Lee *et al.* [21] in a normally magnetized film with an oppositely magnetized tip. In that study, images obtained by scanning a localized mode through an inhomogeneous film yielded a resolution estimate of 200 nm.

At a conceptual level, localized precession in ferromagnets reflects a competition between the local field conditions and the effectiveness of spin-spin interactions in coupling precession energy away into the surrounding film [23]. Spin wave dispersion relations plotted in Fig. 1(a) for the in-plane magnetized film (dark lines) and the normally magnetized film (dashed lines) allow a comparison of the relative strengths of interactions for spin waves that propagate perpendicular or parallel to the static magnetization. At low k, the group velocity is determined almost completely by dipolar interactions, while exchange interactions play a role at the higher k values. The much lower group velocities for $\mathbf{k} \parallel \mathbf{M}$ reflect interactions that are effectively much weaker than for $\mathbf{k} \perp \mathbf{M}$ propagation. In this Letter we describe measurements and modeling of localized spin wave modes in a tangentially magnetized film, compare localization between directions with high and low group velocities, and we estimate the resolution that may be achieved by using these localized modes as local ferromagnetic resonance probes.

We use the magnetic tip of a ferromagnetic resonance force microscope (FMRFM) both to create localization conditions, and to detect the localized resonances. The FMRFM technique combines aspects of magnetic force microscopy (MFM) and ferromagnetic resonance (FMR) to obtain high spatial and spectroscopic resolution [24–26]. Our FMRFM setup centers on a small magnetic tip mounted on a micro-cantilever that is positioned above a sample [Fig. 1(b)]. An external magnetic field $\mathbf{H}$ aligns the magnetization of tip and sample in the sample plane. This field orientation contrasts with earlier FMRFM work which was done with the field normal [19,21,22,24,25], or near normal [20] to the film. The sample is mounted on a stripline that generates a microwave field $\mathbf{H}_1$ perpendicular to $\mathbf{H}$. For microwave frequencies near the ferromagnetic resonance frequency, $\mathbf{H}_1$ drives precession of the sample spins, and the resulting change in the static component of the sample magnetization changes the force between the tip and sample, causing a change in cantilever deflection, which generates the detected signal [Fig. 1(c)].

The experimental details of the setup include a silicon cantilever with a nominal spring constant of 0.1 N/m and resonance frequency of roughly 9.3 kHz. The magnetic tips are fabricated through electron-beam induced deposition

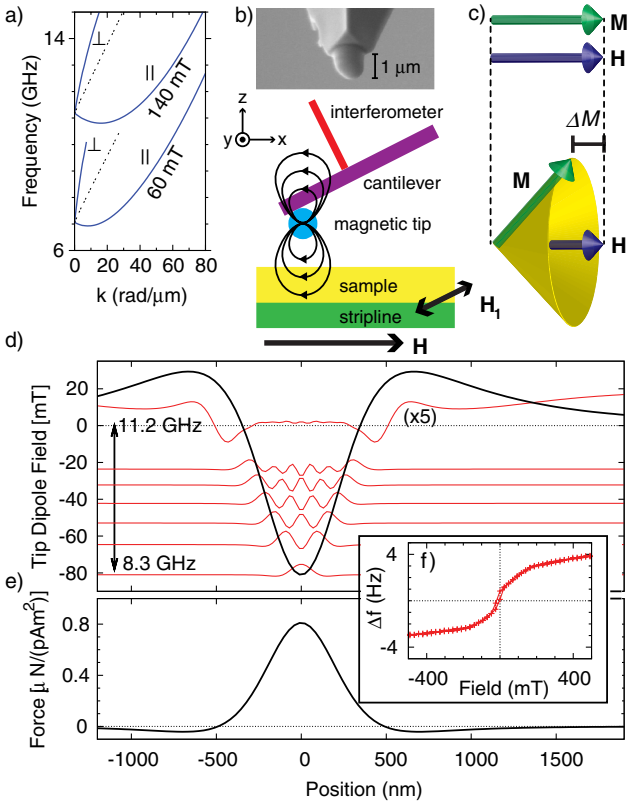

FIG. 1 (color online). (a) Infinite-film spin wave dispersion relations for the minimum field (60 mT) and the externally applied field (140 mT). Solid lines are for in-plane magnetization and dashed lines are for a perpendicularly magnetized film. (b) Schematic setup for FMRFM. A soft ferromagnetic probe on a cantilever generates a low-field region within the sample. Inset: SEM image of electron beam induced deposited (EBID) tip on cantilever. (c) When precession is excited, the quasistatic components of the sample magnetization are reduced, which changes the force between the sample and the magnetic tip. (d) Profile of the field near a soft 1 μm diameter tip (thick line). Thin red lines are modeled profiles of several trapped spin wave modes described in the text. (e) The force on the tip due to a (1 pA m^2) $\hat{\mathbf{x}}$ point dipole as a function of its position on the x axis. (f) Magnetometry of the tip moment showing that the tip is unsaturated below 200 mT.

(EBID) with approximate dimensions of 1.1 μm $\times$ 1.1 μm $\times$ 1.05 μm. The composition of the tip by atomic percentage is 73.7% cobalt, 16.9% carbon, and 9.4% oxygen determined through energy-dispersive x-ray spectroscopy (EDS) with a one-sigma uncertainty of 1%. Planar devices deposited by this technique demonstrate soft magnetic properties with an out-of-plane saturation field similar to that of pure cobalt films [27].

We characterized the tip magnetization curve using a form of cantilever magnetometry. We pass a dc current through the waveguide to create a field gradient. The effective change in the cantilever spring constant is $\delta k = \mu_0 m(H)[d^2H/dz^2]$, and the cantilever's resonant frequency shifts by $\delta f = f\delta k/(2k)$. The resulting frequency change is plotted in Fig. 1(f) as a function of applied field. It is clear from this plot that the magnetization is not saturated for fields less than 200 mT.

The sample film was deposited by electron-beam deposition of a 20 nm Al_2O_3 underlayer on a silicon wafer followed by 20 nm of $Ni_{80}Fe_{20}$. Samples cut from the wafer were then polished from the back side down to a thickness of $\approx$ 50 μm and mounted face up on a strip line with a center conductor width of 50 μm. Measurements were performed at ambient temperatures under vacuum.

The signal was obtained by reflection from a low-finesse optical cavity formed between the cantilever and an optical fiber. A phase locked loop (PLL) tracked the cantilever resonance and supplied a modulation signal to the microwave generator at the cantilever resonance frequency [25]. Modulation of the microwave power results in a cantilever oscillation amplitude consisting of a resonant component that reflects excitation of the sample magnetization and a background signal which we hypothesize may be due to modulated microwave heating of the strip line, substrate and cantilever. Typical cantilever oscillation amplitudes were on the order of 20 nm and a lock-in time constant of 1 s was used.

Figure 2(a) shows the results of measurements at an excitation frequency of 8.1 GHz for tip-sample separations h ranging from 100 to 400 nm. The separation h is measured from the surface of the sample to the bottom of the tip. As a function of applied field, the spectra indicate an attractive force on the low-field side and a repulsive force on the

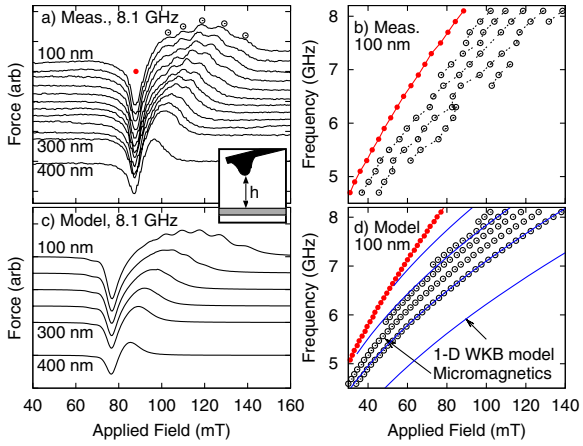

FIG. 2 (color online). (a) FMRFM spectra taken at 8.1 GHz for tip sample separations ranging from 100 to 400 nm in 20 nm increments up to 300 nm. The empty dots represent the position of the localized modes at h = 100 nm while the red dot represents the extended film mode. (b) Peak positions determined by fitting the force spectra in a) for a range of excitation frequencies. Uncertainty estimates from the fit are on the order of 0.1 mT [28]. Corresponding modeled spectra and peak positions are shown in (c) and (d). The solid lines are the results of a 1D WKB model of the spin wave localization.

high-field side. The negative, low-field portion of the signal does not depend strongly on the tip separation. In contrast, the positive, high-field portion shifts in field as the tip is brought closer and several peaks become resolved.

Profiles of the dipole field [Fig. 1(d)] and of the point-dipole response function in [Fig. 1(e)] allow a qualitative explanation of the form of the signal. Here we have assumed a soft, 1 μm diameter, spherical tip, at a height $h = 100$ nm, an applied field $\mu_0 H_0 = 140$ mT. We model the tip as an unsaturated, magnetically soft sphere, so that $M = 3H_0$ for fields below saturation, resulting in a tip moment of 0.175 pA m^2 at 140 mT. The tip force exerted by a (1 pA m^2)$\hat{\mathbf{x}}$ point dipole is calculated for different dipole locations in the sample plane. The strong correlation of repulsive (positive) forces with negative tip fields near the tip and attractive (negative) forces to the sides of the tip suggest that the positive force signal is largely due to precession under the tip and negative signals are due to precession in distant parts of the film.

For small tip-sample separation we observe several peaks within the positive response. We show below that these peaks represent the different localized spin wave modes that exist within the field well. At 100 nm tip-sample separation we observe 5 different modes as indicated with circles in Fig. 2(a). In order to further elucidate the nature of these resonances, we set the tip at 100 nm above the surface and took spectra at different frequencies. We fit the positive portions of the signals in Fig. 2(a) to sums of Lorentzians, and the resulting resonance fields are shown in Fig. 2(b). In the plot we observe five independent localized modes plus the extended film mode with the rightmost mode representing the highest field mode in Fig. 2(a). With uncertainty estimates from the fit on the order of 0.1 mT [28], we attribute the evident waviness in the data to variations of the tip-sample separation from 100 nm.

To interpret these measurements we performed micromagnetic modeling using object oriented micromagnetic framework (OOMMF)[29], approximating the extended film with a 20 μm diameter disk, 20 nm thick, with magnetization $M = 800$ kA/m. The damping parameter α in the disk was changed smoothly from 0.01 to 1.0 in the 2 μm wide rim of the disk in order to suppress possible spin wave reflections from the disk boundary. In addition to a uniform applied field, the model included the field due to an unsaturated 1 μm diameter tip, with magnetization $M = 3H_0$, as described above.

Each force spectrum was calculated from the magnetic response to a short field pulse. The response was recorded in a series of magnetization "snapshots" at 20 ps intervals. For each cell, the power spectra, $S_{M_y}(f, x, y)$ and $S_{M_z}(f, x, y)$ were calculated from the y and z components of the magnetization. Finally, the local, static magnetization change $\Delta M_z(f, x, y) \propto -[S_{M_y}(f, x, y) + S_{M_z}(f, x, y)]$ was weighted by the point response function for dipole-dipole forces and the tip force was calculated as the sum of the force contributions from all the cells.

Figure 2(c) shows the modeled spectra for varying tip-sample separation. The modeled spectra exhibit a similar shape and contain the same number of localized modes as our experimental spectra, confirming most of our experimental results.

Figure 2(d) shows the modeled resonance fields for both the extended film mode and the localized modes. We see excellent agreement between the modeled and experimental spectra. Similar to the experimental spectra not all of the localized modes span the entire frequency range since some modes will merge with others at lower frequency.

From the micromagnetic simulations, we have also generated two dimensional maps of the localized spin wave modes, shown in Figs. 3(a)–3(g), which correspond to the labeled force extrema in Fig. 3(h). Broadly speaking, for the trapped modes, "a"–"f", the precession is largest under the tip, with localized modes taking the form of standing waves in the x direction with lens-shaped wave fronts. For mode "g", precession is small under the tip and large in the extended film.

The close resemblance between the simulated mode structures and planar standing waves suggests that a 1D model of the spin wave modes may be possible. We use a Wentzel-Kramers-Brillouin (WKB) approximation, making use of the infinite-film dispersion relations plotted in Fig. 1(a) for $\mathbf{k} \parallel \mathbf{M}$. The WKB approximation assumes that the field varies slowly compared to a wavelength, so that one can calculate a local value of k for different

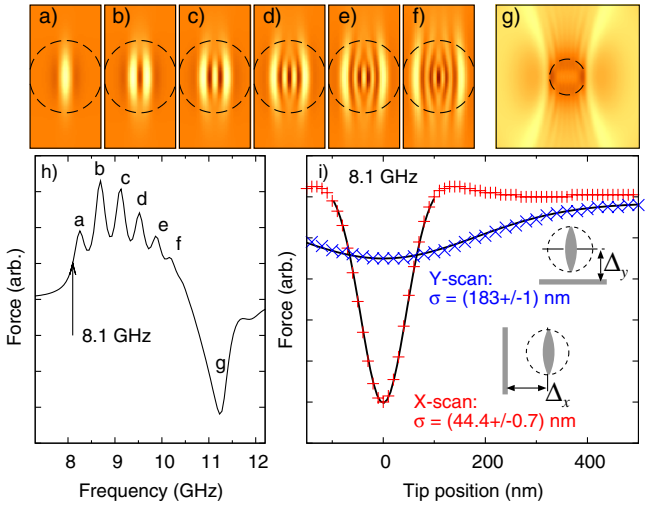

FIG. 3 (color online). Profiles of trapped spin wave modes determined by micromagnetic modeling. Panels (a)–(g) show the mode structures that correspond to the labeled extrema in the modeled cantilever force spectrum shown in panel (h). The dashed circles in (a)–(g) indicate the size of the 1 μm diameter spherical tip. Panel (i) shows the modeled cantilever force as the tip is scanned over 20 nm wide "line defects" where the applied field is 10 mT higher.

combinations of local applied field and excitation frequency. Following Jorzick *et al.* [12], we calculate a phase change $\Delta\phi$ between the center of the field well and a "turning point," x_{turn} where the local field is high enough that the spin wave dispersion relation yields no real-valued solution for k [12,13]. The quantization condition is

$$\Delta\phi = \int_0^{x_{\text{turn}}} k(x, H_0, f)dx = n\frac{\pi}{2}. \quad (1)$$

In Fig. 2(d), we plot field-frequency combinations that satisfy the quantization condition as solid lines. The field mode frequencies obtained by this method follow a field dependence that is similar to the micromagnetic results, but the WKB frequencies are clearly more widely spaced. Only modes with odd n are plotted; even n correspond to modes with odd symmetry that would not be excited by a uniform driving field.

The WKB predictions provide only a qualitative understanding of the trapped spin wave modes. In approximating a 2D field well with a 1D section through the deepest part of the well, the overall strength of the well is overestimated. Further, an underlying assumption of the WKB model is that the field (potential) well varies slowly compared to the wavelength of the spin waves, and this assumption is clearly violated in the present case.

We estimate resolution that may be obtained by scanning the localized mode through defects. We modeled the line defects as thin strips, 20 nm in width where the anisotropy field is 10 mT, easy axis parallel to the applied field. Figure 3(i) plots the tip force at 8.1 GHz as a function of distance Δ from the line defects for x and y scans of the tip. Fits of the central extrema of these scans to $a + b\exp(-\Delta^2/2\sigma^2)$. yield values $\sigma_x = 44.4 \pm 0.7$ nm and $\sigma_y = 183 \pm 1$ nm. The experimental method of Ref. [21] yields a resolution $R = 2.13\sigma$ in the case of a Gaussian response function and a sample with a white noise spatial spectrum. Adopting this ratio as our definition of resolution, we estimate $R_x = (94.5 \pm 1.5)$ nm and $R_y = (390 \pm 2)$ nm [28].

For a model-to-model comparison, we also modeled resolution for the experiment described in Ref. [21] where the field and magnetization are normal to the film, and the circular symmetry is preserved. Using parameters from Ref. [21] we verified the dependence of the localized modes on tip height, and similarly modeled the tip force as a function of position relative to a line defect. We obtain $\sigma = (132.6 \pm 0.6)$ nm, or $R = (282 \pm 1)$ nm [28], a value that falls between the R_x and R_y values described above.

Qualitatively, the contrast between the weak confinement in the y direction and the strong confinement in the x direction can be understood as a consequence of the anisotropy of magnetostatic interactions that occurs with in-plane magnetization. This interaction anisotropy is reflected in the spin wave dispersion relations plotted in Fig. 1(e) for $\mathbf{k} \parallel \mathbf{M}$ (x direction) and $\mathbf{k} \perp \mathbf{M}$ (y direction).

In summary, we have used in-plane magnetic fields to detect and generate multiple localized spin wave modes in an extended film. We have modeled 2D maps of the spin wave modes and proposed how these may be used to image within magnetic nanostructures with nanometer-scale spatial resolution.

We are grateful for the assistance of Meng Zhu for sample fabrication and E. D. Dahlberg and P. C. Hammel for valuable discussions. This work has been supported in part by the NIST-CNST/UMD-Nanocenter Cooperative Agreement.

*hanjong.chia@nist.gov
†robert.mcmichael@nist.gov

[1] S. S. P. Parkin, M. Hayashi, and L. Thomas, Science **320**, 190 (2008).
[2] S. A. Wolf, J. Lu, M. R. Stan, E. Chen, and D. M. Treger, Proc. IEEE **98**, 2155 (2010).
[3] S. Kurtz, E. Varga, M. J. Siddiq, M. Niemier, W. Porod, X. S. Hu, and G. H. Bernstein, J. Phys. Condens. Matter **23**, 053202 (2011).
[4] D. A. Allwood, G. Xiong, C. C. Faulkner, D. Atkinson, D. Petit, and R. P. Cowburn, Science **309**, 1688 (2005).
[5] V. V. Kruglyak, S. O. Demokritov, and D. Grundler, J. Phys. D **43**, 264001 (2010).
[6] T. Schneider, A. A. Serga, B. Leven, B. Hillebrands, R. L. Stamps, and M. P. Kostylev, Appl. Phys. Lett. **92**, 022505 (2008).
[7] A. Khitun, M. Bao, and K. L. Wang, J. Phys. D **43**, 264005 (2010).
[8] Y.-S. Yu, H. Jung, K.-S. Lee, P. Fischer, and S.-K. Kim, Appl. Phys. Lett. **98**, 052507 (2011).
[9] P. Laterbur, Nature (London) **242**, 190 (1973).
[10] S. M. Rezende and A. Azevedo, Phys. Rev. B **44**, 7062 (1991).
[11] S. Demokritov, J. Phys. Condens. Matter **15**, S2575 (2003).
[12] J. Jorzick, S. O. Demokritov, B. Hillebrands, M. Bailleul, C. Fermon, K. Y. Guslienko, A. N. Slavin, D. V. Berkov, and N. L. Gorn, Phys. Rev. Lett. **88**, 047204 (2002).
[13] J. P. Park, P. Eames, D. M. Engebretson, J. Berezovsky, and P. A. Crowell, Phys. Rev. Lett. **89**, 277201 (2002).
[14] B. B. Maranville, R. D. McMichael, S. A. Kim, W. L. Johnson, C. A. Ross, and J. Y. Cheng, J. Appl. Phys. **99**, 08C703 (2006).
[15] B. B. Maranville, R. D. McMichael, and D. W. Abraham, Appl. Phys. Lett. **90**, 232504 (2007).
[16] R. D. McMichael, C. A. Ross, and V. P. Chuang, J. Appl. Phys. **103**, 07C505 (2008).
[17] M. Zhu and R. D. McMichael, J. Appl. Phys. **109**, 043904 (2011).
[18] H. T. Nembach, J. M. Shaw, T. J. Silva, W. L. Johnson, S. A. Kim, R. D. McMichael, and P. Kabos, Phys. Rev. B **83**, 094427 (2011).
[19] Y. Obukhov *et al.*, Phys. Rev. Lett. **100**, 197601 (2008).

[20] E. Nazaretski, D. V. Pelekhov, I. Martin, M. Zalalutdinov, D. Ponarin, A. Smirnov, P. C. Hammel, and R. Movshovich, Phys. Rev. B **79**, 132401 (2009).
[21] I. Lee, Y. Obukhov, G. Xiang, A. Hauser, F. Yang, P. Banerjee, D. Pelekhov, and P. Hammel, Nature (London) **466**, 845 (2010).
[22] I. Lee, Y. Obukhov, A. J. Hauser, F. Y. Yang, D. V. Pelekhov, and P. C. Hammel, J. Appl. Phys. **109**, 07D313 (2011).
[23] R. D. McMichael, D. J. Twisselmann, and A. Kunz, Phys. Rev. Lett. **90**, 227601 (2003).
[24] Z. Zhang, P. C. Hammel, and P. E. Wigen, Appl. Phys. Lett. **68**, 2005 (1996).
[25] O. Klein, G. de Loubens, V. V. Naletov, F. Boust, T. Guillet, H. Hurdequint, A. Leksikov, A. N. Slavin, V. S. Tiberkevich, and N. Vukadinovic, Phys. Rev. B **78**, 144410 (2008).
[26] P. C. Hammel and D. V. Pelekhov, in *Handbook of Magnetism and Advanced Magnetic Materials* (John Wiley & Sons, Ltd., New York, NY, 2007), Vol. 5.
[27] L. M. Belova, E. D. Dahlberg, A. Riazanova, J. J. L. Mulders, C. Christophersen, and J. Eckert, Nanotechnology **22**, 145305 (2011).
[28] Uncertainties are 1 standard deviation estimated through the least-squares fit. Uncertainties in modeled results do not reflect uncertainty in the model parameters.
[29] M. J. Donahue and D. G. Porter, in *Interagency Report NISTIR 6376* (National Institute of Standards and Technology, Gaithersburg, MD, 1999).